Peer-reviewed version available at Colloids Interfaces 2018, 2, 52; doi:10.3390/colloids2040052

Article

Photoluminescence Property of Eu^{3+} Doped $CaSiO_3$ Nano-Phosphor with Controlled Grain Size

Boris B. Niraula *, Conrad Rizal

SeedNanoTech and Consulting, Brampton, ON, Canada L6Y 3J6.
*Correspondence: boris.niraula@seednanotech.com

Abstract: A series of Eu^{3+} doped $CaSiO_3/SiO_2$ nano-phosphor powder of controlled grain size, crystalline structure, and chemical composition were synthesized using the microemulsion technique. XRD profiles of samples sintered over 600 of suggested phase shift from amorphous powder grain to more ordered polycrystalline powder of triclinic type wollastonite, $CaSiO_3$, with preferred crystal phase orientation of (112) and tetragonal type cristobalites of SiO_2. The grain size, crystallinity, and chemical composition of the host matrix, activator and sensitizer strongly affected both the absorption and emission bands of these samples. The amplitude of both the orange and red emission bands significantly increased with sintering temperature. The emission band is red-shifted with decreasing grain sizes. These bands displayed good sensitivity to ionic concentration of the Si^{4+}, Ca^{2+}, and Eu^{3+}. With increasing Ca^{2+} ion concentration both the intensity of the red photoluminescence (PL) band increased and a concentration quenching observed. Increase in Si^{4+} ion concentration led to quenching in PL intensity of both the orange and red bands whereas the amplitude of the blue-band slightly increased. With increasing Eu^{3+} ion concentration the red-band initially increased whereas it started decreasing at higher sample concentration. In the presence of Ca^{2+} ion as a sensitizer, the sample showed a remarkable PL property—including—about 100% photon conversion efficiency and a two-fold increase in excitation and emission photons.

Keywords: polycrystalline nano phosphor, photoluminescence, Eu^{3+} doped $CaSiO_3$, microemulsion technique

1. Introduction

Eu^{3+} doped phosphors employed in lighting and display technologies such as electroluminescence cells, plasma display panels, high-efficiency fluorescent lamps, light emitting diodes, and waveguides as they show remarkable photoluminescence properties [1]. In pure form, Eu^{3+} ions show emission lines extending from visible to near infra-red domain of the electromagnetic spectrum. These ions usually absorb photons from 200 nm to 270 nm and emit orange and red lines in the visible region. A phosphor that absorbs photons in this domain is suitable for making display panels and fluorescent lamps [2]. However, absorption of Eu^{3+} in the UV region is weak, and such a phosphor are not suitable in making light emitting diodes (LED). By adding Eu^{3+} as a dopant into a host matrix such as SiO_3 and in the presence of rare earth ions as sensitizers, the luminescence property of this phosphor can, however, enhance substantially. When used as a dopant in a glass matrix, the Eu^{3+} ions, however, show absorption and emission bands instead of absorption and emission lines. The peak positions and intensities of these bands bear a strong relationship with the size distribution of the crystal grain, their chemical composition, and morphology. Earlier reports have shown that crystal grain size, their distribution, resistance to particle agglomeration, and spherical morphology are the most critical factors for a phosphor to have good luminescent characteristics [3, 4].

In the past techniques such as solid-state chemistry [3] and ion implantation [4] have been the sole means of synthesizing phosphor material. Today these techniques are becoming unpopular for several considerations. These include high production cost and poor product quality as identified by weak PL efficiency and poor non-linear optical effects. The problem is that these methods are energy intensive as the mixing of activator and sensitizer ions with the host are carried out at and around melting temperature of the host matrix. It means the viscous nature of the melt does not allow to have a homogenous mixing of the activator ion, and the glass matrix is impossible to achieve.

Another inherent problem is that phosphor particles and crystallite grains tend to precipitate upon cooling, and this process accompanies agglomeration of particles that is induced by inter-ionic interaction. The result is production of low quality, poorly homogenized phosphor not suitable for the most optoelectronic application. These, in turn, suggest that the possibilities of improving the quality of PM are a cumbersome job when robust state methods are employed, whereas the new developments in display and other technologies such as light amplifiers and wave-guides require drastic improvement in PL efficiency and non-linear optical properties [5]. The need to reduce production cost.

The solutions to these problems have been addressed using rather simple solution-based synthesis techniques such as sol-gel and micro-emulsion, and these techniques are gaining widespread popularity for the past few decades [6-8]. Also, these techniques make use of simple room temperature hydrolysis and polycondensation reaction [9, 10] of the starting material such as *tetraethylorthosilicate* (TEOS), yielding glasses and oxide powders of high purity and homogeneity and to some degree with tailored grain size, morphology, and dispersity index.

A large number of reports suggest that the PL properties of the phosphor strongly depend on the composition of the glass matrix, crystal structure and grain size of the crystallites [11, 12]. For example, the reduction in grain size often leads to significant improvement in luminescence efficiency and non-linear optical effects [13]. Interestingly, the increase in luminescence efficiency is reported to be accompanied by a decrease in absorption intensity and redshift in both the absorption and emission bands. For these reasons, for the past decade, the exploration of size-dependent properties of the phosphor has been a subject of scrutiny. This work reports on how the photoluminescence property of Eu^{3+} doped nano phosphor is affected by factors such as the composition of glass matrix, dopant concentration, the average size of crystals and sintering temperature as well as on how particle size of the powder can be controlled and tailored using emulsion technique.

The excitation and emission bands of Eu^{3+} ion are broad due to the transition of electrons between the $^4F_7$ ground state and the crystal field component of the $^4F_6 \rightarrow {}^5D_7$ excited state configuration [14]. Luminescence band is observed either from excitonic emission, also referred to as recombination of an electron-hole pair, or from the radiative relaxation of the trap states [15]. While excitonic emission is characterized by narrow, near absorption edge luminescence, the trap-state emission is characterized by broad, strong red-shifted luminescence that sometimes exhibits multiple bands, also referred to as band splitting. The electron-hole pair results from the absorption of a photon.

The problem is that with the decrease in size, the photoluminescence may show an increasing number of defect sites as the surface-to-volume ratio increases with decreasing particle size. The rising defects result in rapid trapping of either the electron or the hole and lead to localization of charged site at the surface [16, 17].

In literature, a wide variety of sensitizers have been used to enhance the photoluminescence efficiency of the silica-based phosphor. However, the problem is that the energy transfer from the sensitizer to Eu^{3+} has been minimal. This work utilizes Ca^{2+} as a sensitizer since the energy transfer from Ca^{2+} to Eu^{3+} is accompanied by endothermic charge transfer reaction, leading to dramatic

enhancement in photoluminescence property of the nano-phosphor - including a two-fold increase in photon absorption and emission and 100 % quantum efficiency for a down-conversion phosphor.

2. Materials and Methods

Reagent grade cyclohexane of 99.5% purity was used as an oil phase. $Ca(NO_3)_2$ was used as sources of Ca^{2+} ions, and these were of 99 % purity. The anionic surfactant used was Triton X-45, and it was of analytical grade. It usually comes as a poly-dispersed preparation of tetra-methyl-butyl-phenyl-poly-oxyethylene with an average of 5 oxyethylene groups per molecule. The source of silica glass precursor was TEOS (tetra ethoxy silicate). All these were purchased from *Fluka*. The dopant used was $Eu(NO_3)_3$ of 99.9 % purity, and it was purchased from Sigma-Aldrich. Ammonium hydroxide (solution of 25 % NH3) was used as a hydrolytic agent, and it was of reagent grade. Absolute ethanol, 99.8 % purity (*HmbG GmbH, Germany)* was employed to clean the glassware used in this work. The deionized water used was from *Millipore system* with an ionic conductivity of 18 μS / cm.

The morphology, size, and shape of the synthesized phosphor powder were analyzed using a Philips CM12 Transmission Electron Microscope (TEM). The particle size of the sample was also measured using Coulter counter N_4 plus photo correlation spectroscopy. The crystal structure and their phase composition were analyzed using Rigaku RINT-1400 X-ray diffraction *(Rigaku, Tokyo Japan)* system. This system is supplied with a Cu Kα radiation source of 40 kV and 100 mA. Both the PL and photoluminescence excitation spectra were scanned using a PERKIN ELMER LS 50B luminescence spectrometer *(PERKIN ELMER LS 50B, UK).* Thermal analysis was carried out using Mettler Toledo made thermos gravity metric analyzer (TGA). As far as curing is concerned, the sol-gel reaction was carried from 100^{o}C to 1000^{o}C under neutral gas atmosphere with a heating rate of 10^{o}C /minute, whereas the gas flow rate was maintained at 120 cm^3/ minute.

As described above, the Eu^{3+} ion doped $CaSiO_3$ and $MgSiO_3$ phosphor powder were prepared using the microemulsion technique, whereby TEOS is used as the glass precursor. Two types of water-in-oil (w/o) micro-emulsion systems were prepared separately. These can be referred to as w/o system 1 and w/o system 2. Both systems contained three common components, viz., the surfactant, TEOS, and cyclohexane as the continuous phase. Both systems contained 15 wt % surfactant, 82.46 wt % of cyclohexane, 1.54 wt % of TEOS and one wt % of the aqueous solution. The only difference between system 1 and 2 was that system 1 contained 3.0 M calcium nitrate with varying concentration of europium nitrate, whereas system 2 included a solution of 0.5 M ammonium hydroxide.

The water-to-surfactant molar ratio is also denoted as R_o from now on. By varying total water concentration, the R_o value of samples was varied. In this case, the R_o value of emulsions was changed from 0.12 to 0.3 as the average grain size of the crystallite, which is obtained because of hydrolysis and condensation reaction of TEOS, appears to depend mainly on R_o value of the emulsion system from which they are prepared. The detail of which is given elsewhere, and it will not be discussed here. Note, in any case, while varying the value of R_o the overall concentrations ratios of ethanol, surfactant and TEOS is kept constant. Next, equal amounts of system 1 and 2 were mixed in a third container, which in its turn under-went continuous stirring for 24 hours. At the end of 24 hours, this would give Eu^{3+} ion doped dispersion of $CaSiO_3$/ and SiO_3 phosphor. This procedure naturally yields PM with nanometer-sized grains, whereby the grain size is primarily defined by the R_o value of the emulsion used during synthesis.

Next, for removing the oil phase (cyclohexene in this case) and surfactant, the dispersed phosphor is then washed five times with ethanol. These particles are then collected and dried at 200 ^{o}C for two hours followed by sintering at 400 ^{o}C to 800 ^{o}C for 3 hours. Note, the heat treatment is designed to remove any residue of surfactant, water, and oil from the sample. The given samples

were calcinated at a temperature ranging from 400 °C to 800 °C, as the grain size of the phosphor is also affected by curing conditions.

3. Results and Discussions

3.1 Microstructure Analysis

We investigated the microstructure of phosphorous power using transmission electron microscopy (TEM). The TEM images of the as-synthesized nano phosphor powders with R_o = 0.12 to 0.30, are depicted in Fig. 1. These images indicate that grain size of the phosphor depended strongly on R_o value of the micro-emulsion of which they were synthesized: the grain size of the phosphor powder, increased with the increase in R_o value of the microemulsion and vice versa. As can be seen in these TEM images, the phosphor samples under investigation were mono-dispersed regarding grain size distribution and were spherical irrespective of R_o values. These images further suggest that by controlling the size of droplets of the microemulsion, the grain size of the phosphor powder can be controlled with a high degree of accuracy.

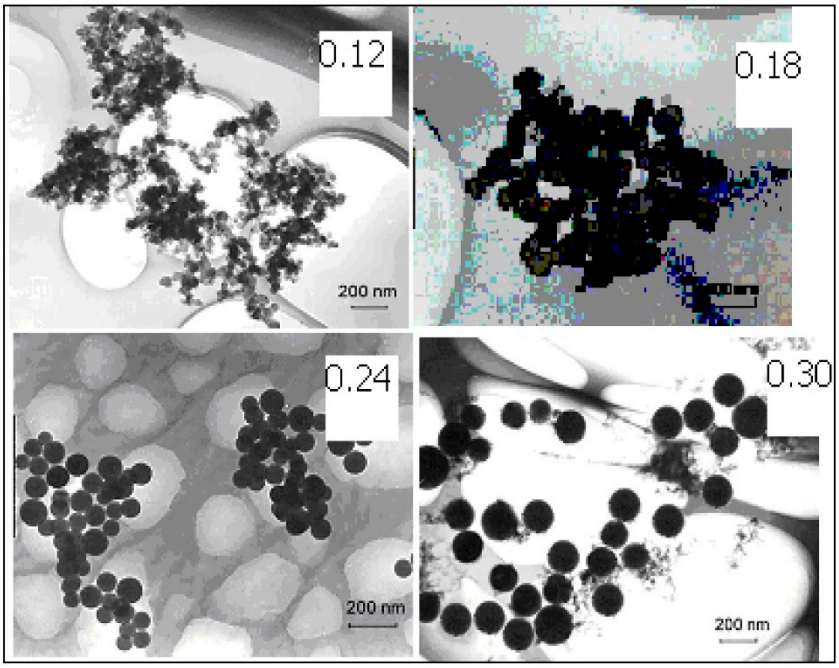

Figure 1. TEM images of Eu^{3+} doped $CaSiO_3$ nano phosphor powder as a function of R_o value of micro-emulsions of which they were prepared at 800 °C.

Light scattering technique was also employed to measure the grain size of the phosphor powder. In this case, *Coulter Counter N4 Plus* was used. R_o value dependent grain size of the phosphor powder is given in Fig 2. As in the case of TEM images, the average grain size and size distribution of the phosphor increased with increasing R_o value of the micro-emulsion of which they were synthesized.

Fig. 3 shows the effect of sintering on grain size. As shown in it, the grain size increased with increasing sintering temperature.

The effect of Eu^{3+} ion concentration on X-ray diffraction, XRD, spectra of the phosphor was studied. **Fig. 4** shows XRD patterns of Eu^{3+} doped wollastonite, $CaSiO_3$ / SiO_3 nano phosphor sintered at 800 °C. Phase analysis indicated that wollastonite type polycrystalline structures dominated these samples. At the same time, tetragonal cristobalite of SiO_2 was also detected in these samples. The wollastonite type crystal orientation is identified with main peaks at 28.8° (-310), 30.0° (112), 36.3°

(400) and 39.11° (-240), and these correspond to the triclinic structure. It means that these samples consist of triclinic type unit cell. The tetragonal cristobalite structure due to SiO_2 is identified with main peaks at 22.0° (101), 28.5° (111), 31.5° (102) and 36.2° (200).

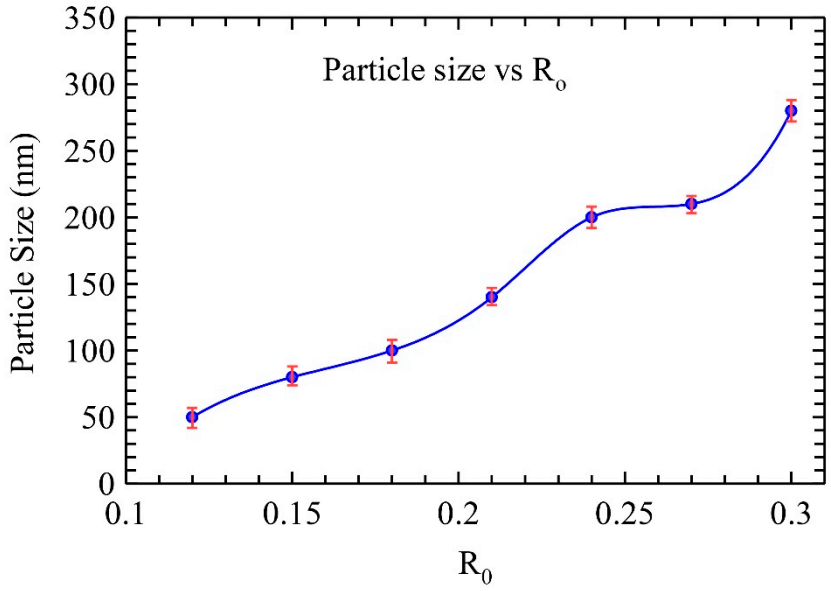

Figure 2. The plot of R_0 value dependent average particle size of Eu^{3+} doped $CaSiO_3$ nano phosphor powder sintered at 800 °C. The data were analyzed using quadratic regression analysis, by utilizing the method of least squares, and fitted with the models generated from the available data, thus ensuring best fits with minimum errors.

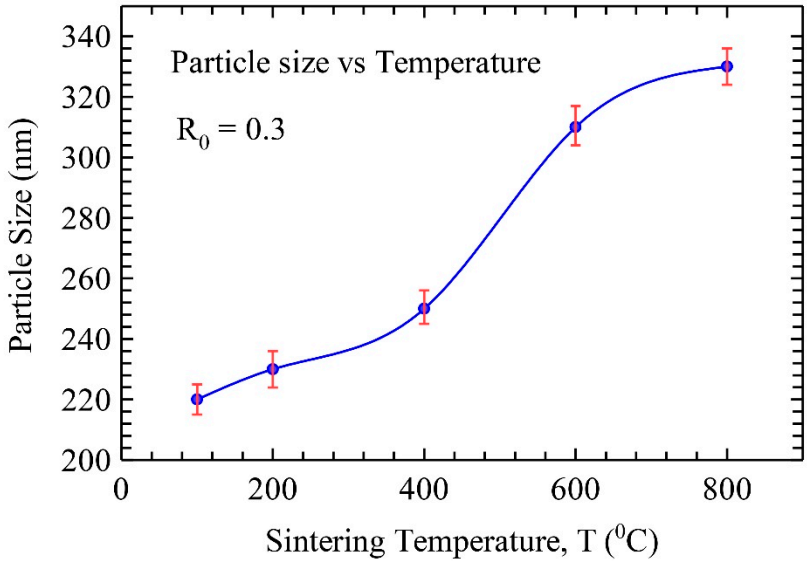

Figure 3. Sintering temperature dependence of grain size distribution of Eu^{3+} doped $CaSiO_3$ nano phosphor powder. The samples were prepared in the presence of an identical concentration of reactants and with a R_o value of 0.30. The data were analyzed using quadratic regression analysis, by utilizing the method of least squares.

The X-ray diffraction (XRD) profiles in Fig 5 shows that the intensity of the XRD peak increased monotonously with intensity ratios of (100) and (101), and (002) and (101) peaks with variation in Eu concentration. The ratio of the peak intensities of (100) and (101) progressively increases from un-doped to 5% of Eu doping. Past 2% of doping, it showed a rather small increase, suggesting the

dopant concentration is nearing saturation. Likewise, the ratio of the intensity of (002) and (101) peaks showed a similar trend. The only difference is being that past 3% of Eu, a concentration quenching effect is observed. The variation in the latter case is though rather small, while the rate of increase with dopant concentration is higher for the former one. As can be seen, the (100) peak is progressively emerging with increasing Eu. A tendency of enhancing polycrystalline nature of SiO_3 films appeared with increasing Eu concentration. Finally, with 5% of Eu doping, the intensities of (100), (002) and (101) peaks are almost the same, and it is a quite interesting point to note. The broadening of peaks with doping concentration seems to be due to the substitution of Si^{4+} ions by Eu ion with comparatively higher ionic radius.

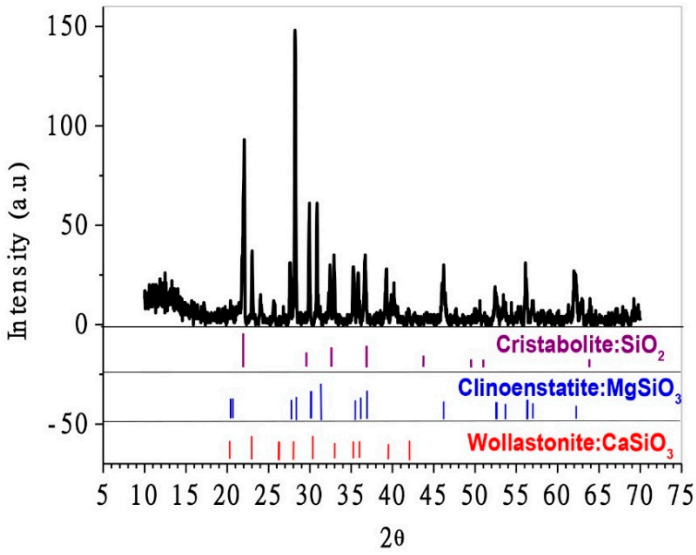

Figure 4. XRD spectrum (Intensity vs. 2θ°) of Eu^{3+} doped $CaSiO_3$ / SiO_3 nanophosphor powder and its crystallinity. Samples were prepared using a R_o value of 0.30 and were sintered at 800 °C.

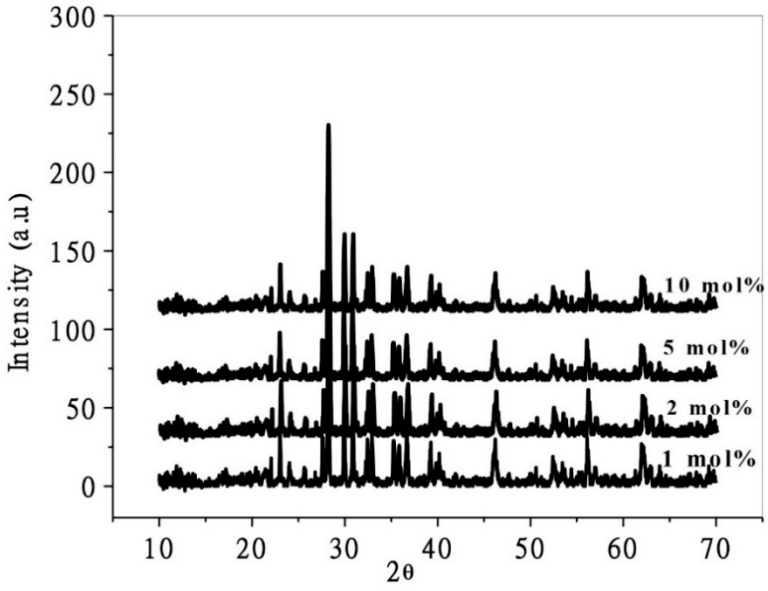

Figure 5. Effect of Eu^{3+} ion concentration on XRD spectrum (Intensity vs. 2θ°) of Eu^{3+} doped $CaSiO_3$ / SiO_3 nano phosphor powder and its crystallinity. Samples were prepared using a R_o value of 0.30 and sintered.

Fig 6 shows that the crystallinity of the phosphor increased with increasing calcination temperature. Sharp peaks in this figure demonstrate that at and below 600 °C the nano powder

sample is amorphous, whereas the peaks at 22.0°, 28.1°, 30.0°, and 31.0° get more defined and more intense when calcinated at 800 °C, suggesting that a distinct crystalline phase develops at this temperature. Also, as can be seen, there is no change in crystal structure when samples sintered at 800 °C, and 1000 °C are compared, suggesting that these samples can be sintered well at 800 °C.

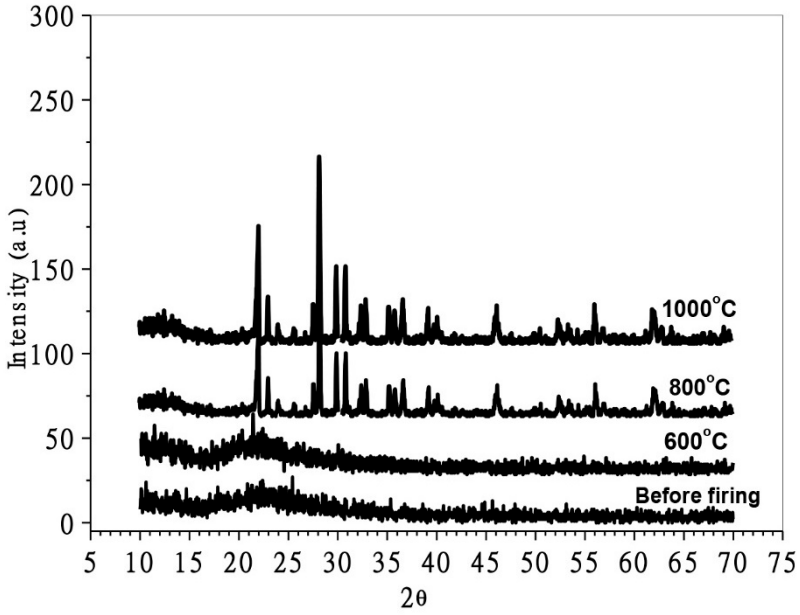

Figure 6. Effect of sintering temperature on XDR spectra (Intensity vs. 2θ°) of Eu^{3+} doped $CaSiO_3$ / SiO_2 nanophosphor powder. Samples were prepared using a R_o value of 0.30 and by keeping the concentration of Ca^{2+} and Si^{4+} and Eu^{3+} in constant.

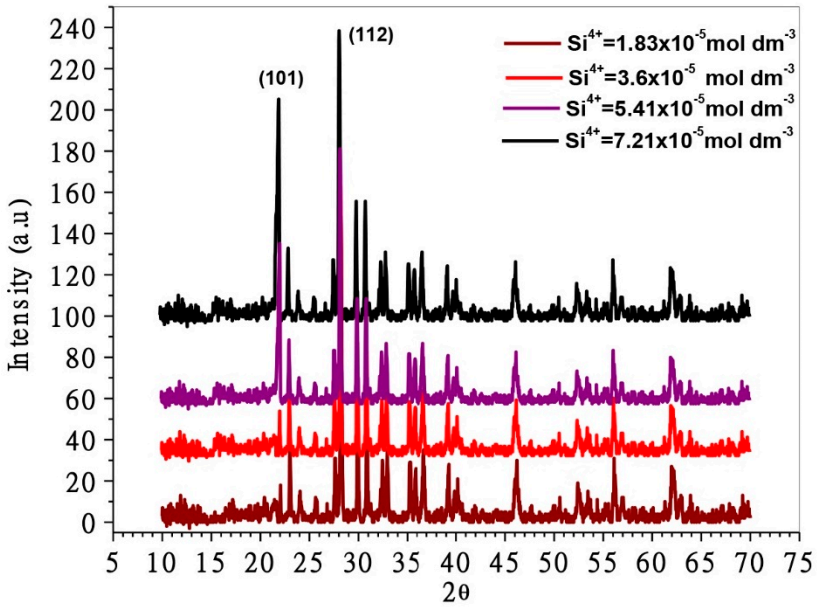

Figure 7. Effect of Si^{4+} concentration on XRD spectra (Intensity vs. 2θ°) of Eu^{3+} doped $CaSiO_3/SiO_2$nano phosphor powder. Samples were prepared in an identical reaction condition using a R_o value of 0.30 and sintered at 800 °C.

Fig. 7 shows the X-ray diffraction spectrum of Eu^{3+} doped $CaSiO_3$ / SiO_2 nano phosphor as a function of silica concentration. In this figure, a small peak that appears at 22.0°, corresponding to (101) plane, at a silica ion concentration of 1.83 $\times 10^{-5}$ mol dm^{-3}, indicates the presence of SiO_2 cristobalite. The intensity of this peak increased with increasing silicon concentration, suggesting that

silica composition strongly influences the crystal structure: increasing Si concentration led to an increase in SiO_2 cristobalite structure with a preferred orientation towards (101).

Fig 8 shows the effect of Ca^{2+} ion concentration on XRD spectra of Eu^{3+} doped $CaSiO_3$/ SiO_2 phosphor powder. These spectrums suggest that Ca^{2+} ion concentration plays a significant role in imparting crystal structure. The preferred crystal orientation is (112) in this case.

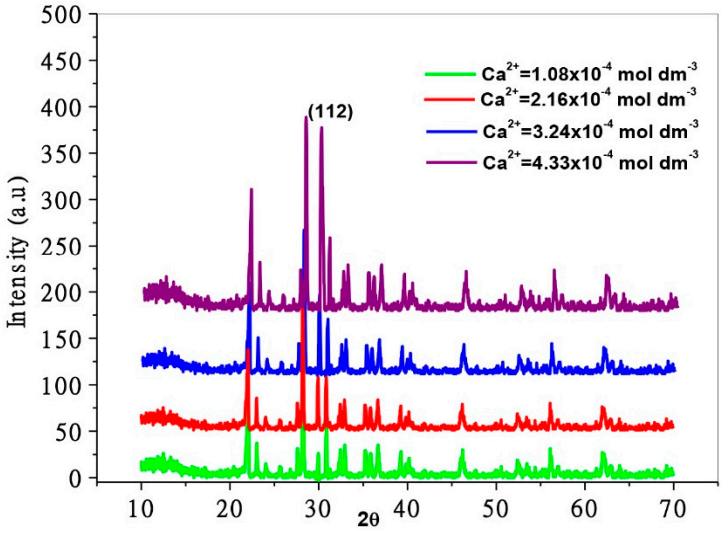

Figure 8. Effect of Ca^{2+} ion concentration on XRD spectra (Intensity vs. 2θ°) of Eu^{3+} doped $CaSiO_3$ / $MgSiO_3$ nano phosphor powder. The samples were prepared in identical condition using a R_o value of 0.30 and sintered at 800 °C.

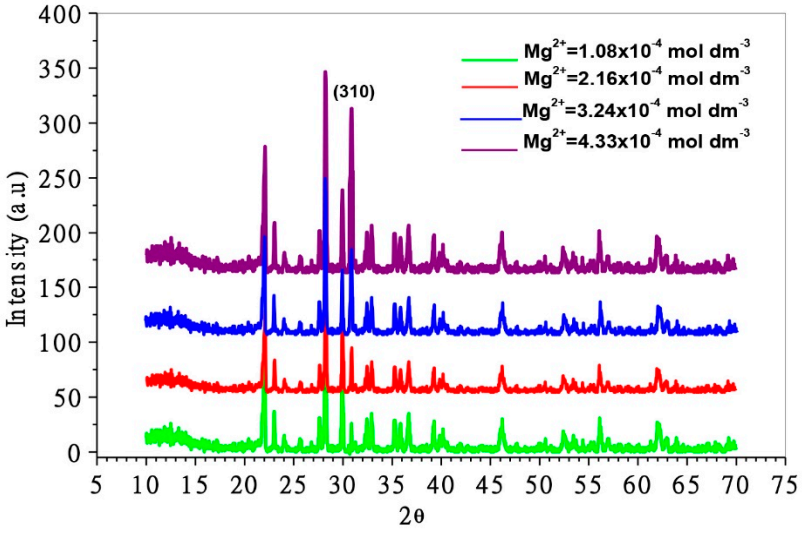

Figure 9. The effect of Mg^{2+} concentration on XRD patterns (Intensity vs. 2θ°) of Eu^{3+} doped $MgSiO_3$ / SiO_2nano phosphor powder. Samples were prepared in identical conditions using a R_o value of 0.30 and sintered at 800 °C.

A similar effect is observed when Mg^{2+} ion concentration is changed as shown in Fig 9. These XRD patterns suggest that the crystallinity of this batch of phosphor also varies with the variation of Mg^{2+} ion concentration. Much like the effect of Ca^{2+} ion, the powder becomes more crystalline with increasing Mg^{2+} ion concentration. However, in this case, the preferred crystal orientation is (310) plane.

3.2 *Photoluminescence Study: Wavelength, Composition, Temperature, and Particle Size*

Eu^{3+} doped $CaSiO_3$ / SiO_2 nano powder showed an absorption band, also referred to as excitation band, resolved at 220 nm and 223 nm, respectively as shown in Fig 10. In accordance to [16], the excitation of Eu^{3+} doped $CaSiO_3$ / SiO_2 can be explained as follows: The energy of the Eu^{3+} charge transfer spectra is closely related to the degree of co-valency of the Eu^{3+}-ligand bond, and this can be explained by considering Eu^{3+} - O^{2-} - Ca^{2+} bonding structure. Since the Ca^{2+} ion is a cation with a smaller radius and larger electronegativity compared to Eu^{3+} ion, the electron density clouding around O^{2-} ion decreases when it is bonded to Ca^{2+} ion. It naturally means more energy is needed to transfer an electron from O^{2-} to Eu^{3+}.

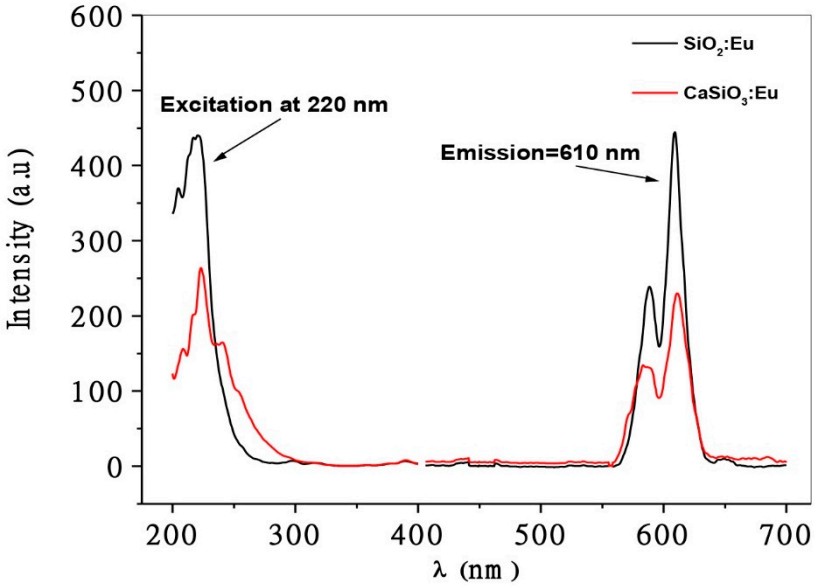

Figure 10. Excitation and emission spectra of Eu^{3+} doped $CaSiO_3$ / SiO_2 nano powder. The concentration of Eu^{3+} ion 5 mol %. Samples were prepared using a R_o value of 0.30 and sintered at 800 ^oC.

With increasing Eu concentration both the band gap as well as the average grain size decrease as reported by *Sun et al.* for Al-doped ZnO film [26] and *Leonyuk et al.* for bulk Eu doped ZnO [18]. According to this model, periodic variations in potential within the grain occurs due to trapping of impurities arising from doping. This periodic variation of potential, in turn, leads to band bending which is identified by a band tailing effect [15, 17, 19]. Impurity band formation is an obvious consequence of increased doping concentration [16] and the trapping of the Eu atoms at the grain boundary usually leads to the introduction of the Eu defect states within the forbidden band.

With increasing Eu doping, the density of the dopant-induced defect states increases, leading to an observed decrease of band gap or redshift. Similar observation of introduction of Eu defect state within the band gap has also been reported by researchers elsewhere. [4, 10, 20].

The trapping of Eu impurities within the grain and the introduction of Eu defect states within the forbidden band gap region are intimately related to the disorder introduced into the system by doping.

The band gap energy (E_g) can be plotted against the inverse of the average grain size (1/D). 1/D depicts the surface to volume ratio of the constituent particle of the sample, and with decreasing grain size, the disorder gradually can increase. Thus, the variation of 1/D with doping concentration can be used as a measure of disorder introduced into the system. It is quite evident that disorder in crystal

lattice should increase with increasing Eu concentration as the ionic radius of Eu is much higher than that of Si.

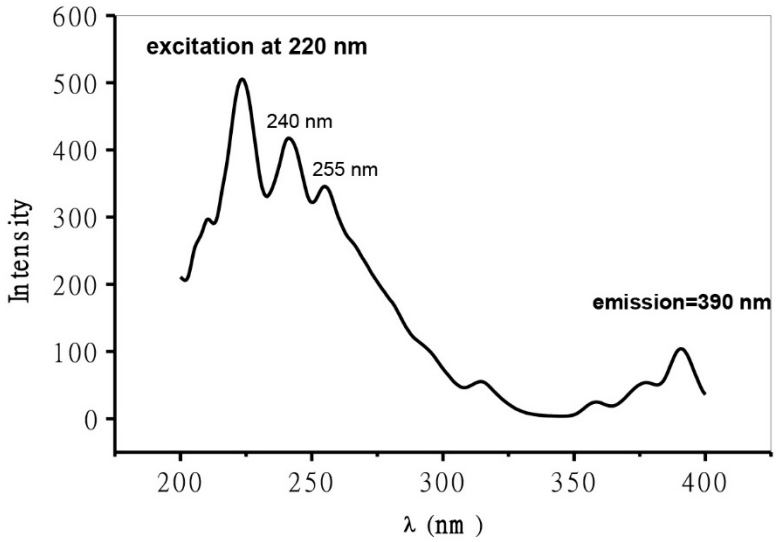

Figure 11. The excitation spectra of Eu^{3+} doped $CaSiO_3/SiO_2$ nano phosphor powder showing a weak blue emission at 390 nm due to direct excitation of the Eu^{3+} ion. The sample was prepared using a R_o = 0.12 and sintered at 800 °C.

A typical spectrum consisting of excitation and emission bands of Eu^{3+} doped $CaSiO_3$ / SiO_3 nanophosphor powder is displayed in Fig 11. In this case, the broadband resolved at ≈ 220 nm is thought to be due to the excitation of the host lattice. Its immediate implication is that the excited host lattice in its turn can transfer the energy to its neighboring activator ion through lattice vibration. The activator ion in its turn absorbs this quantum of energy, because of which it shows two broad excitation bands, peaking at 240 nm and 255 nm, whereas a blue color emission rising at 390 nm accompanies these processes.

Also, a weak emission band is observed at 390 nm when the sample is excited with a 220-nm band. This absorption-emission process corresponds to $^4F_6 \rightarrow {}^5D_1$ transition, within the $^4F_7$ electron configuration of the Eu^{3+} ion. The broad adsorption band resolved at 220 nm is usually assigned to electronic shift involving the transfer of charge from O^{2-} ion ligand to rare earth ion, whereas the emission band at 390 nm is thought to be due to intra-ionic $^4F_6 \rightarrow {}^5D_1$ transition. Note these transitions are assigned based on lanthanide spectra of [21] and [22].

Interestingly, this emission band usually appears at 440 nm [14] for its bulk counterpart, suggesting a robust high energy shift for nanophosphor powder. In this case, the change amounts to 50 nm as the average grain size of the phosphor powder is reduced substantially to the nanoscale, and this shift in emission band can be accounted for the so-called nanosized effect. Note with the bulk counterpart the authors intend to refer Eu^{3+} doped $CaSiO_3$ phosphor powder synthesized using the solid-state method.

In any case, the emission at high energy indicates the fact that the activation energy (kinetic energy) of the valence electrons of the activator ion substantially increases as the particle size of the matrix host decreases. Since higher quanta of energy are needed to excite samples as the particle size decreases [23], it is presumed that band gap energy of these phosphor increases with decreasing grain size, and it can be viewed as a nanosized effect. Given that this assumption is valid, the smaller the average size of the crystallites, the higher the quanta of energy they require to be excited. This consideration naturally leads to the conclusion that the position of excitation band is closely related to the structure of the host lattices and size of their crystallites.

Preprints (www.preprints.org) | NOT PEER-REVIEWED | Posted: 19 September 2018 doi:10.20944/preprints201809.0376.v1

Peer-reviewed version available at Colloids Interfaces 2018, 2, 52; doi:10.3390/colloids2040052

The PL spectrum of the Eu^{3+} doped $CaSiO_3$/ SiO_2 nanophosphor at the excitation energy of 220 nm is given in Fig. 12. Under these conditions, the given phosphor showed a small emission peak centered at ≈ 445 nm, whereas two sharp emission peaks centered at ≈ 580 nm and 600 nm. Note the emission peak at 580 nm, and 610 nm is ascribed to ^5D_o to the $^7F_1$ transition of Eu^{3+}.

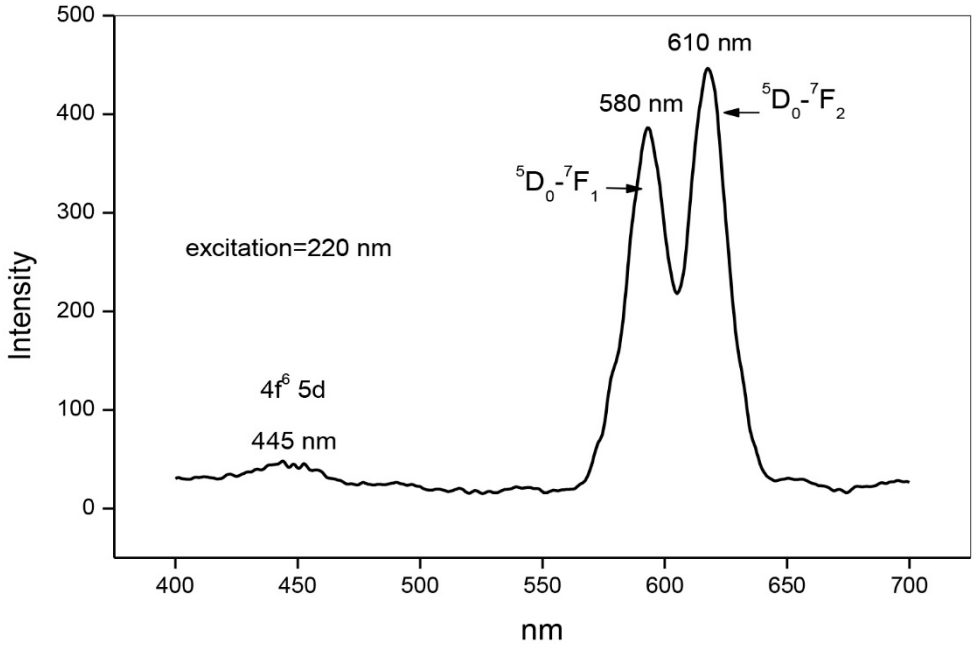

Figure 12. Photoluminescence spectrum of Eu^{3+} doped $CaSiO_3$ / SiO_2 nano phosphor powder at an excitation energy of 220 nm. The sample was prepared using a R_0 value of 0.12 and sintered at 800 °C.

Eu^{3+} ion is characterized by a ^7F ground state electronic manifold, whereas its lowest excited state shows ^5D character with the $^5D_0$ state emitting red light typical of Eu^{3}+ activated phosphor. Also, it is a well-accepted fact that above the ^5D states, closely spaced F orbitals are present, and these are responsible for charge transfer states. Through the absorption of UV, the Eu^{3+} ion gets excited into the charge transfer state, which subsequently relaxes into $^5D_0$ level, emitting red light at 590 nm and 610 nm [24].

It is believed that the main emission peak at 610 nm is due to the electric dipole transition (EDT) of $^5D_o \rightarrow ^7F_2$, whereas the emission peak at 580 nm is thought to be due to magnetic dipole transition (MDT) of $^5D_o \rightarrow ^7F_1$. It is widely known that the $^5D_o \rightarrow ^7F_2$ transition is hypersensitive and it depends strongly on local symmetry, whereas the $^5D_o \rightarrow ^7F_1$ transition is usually insensitivities to site symmetry. These latter two types of developments generally originate from the presence of impurity ion as it cannot occupy the space along the center of symmetry of the crystal lattice, giving both MDT and EDTs [25]. It is also thought that only MDTs are allowed when a rare-earth impurity ion is located at the center of symmetry of a crystal lattice.

Interestingly, as shown in this figure, both the MDT and EDTs, $^5D_0 \rightarrow ^7F_1$ and $^5D_o \rightarrow ^7F_2$, respectively, are observed in this case. For example, the EDT, at ≈ 610 nm probably arises because of lack of inversion symmetry at the Eu^{3+} site. The reason this transition is much stronger than $^5D_o \rightarrow ^7F_1$ transition is that it is usually produced because of the crystal-field splitting of the $^7F_2$ level. On the other hand, the MDT, $^5D_o \rightarrow ^7F_1$, is insensitive to the site symmetry, and the reason why it has appeared here can be due to the lack of center of symmetry in $CaSiO_3$ crystals [26].

On the other extreme, the emission band at 445 nm is usually assigned to $^4F_6 \rightarrow ^5D_1$ excited states due to $^4F_7$ ground state transition, and such a shift gives rise to a blue emission. The appearance of this peak is thought to be due to the presence of monoclinic-$CaSiO_3$ structure [27]. It is supposed that

this band is related to a variety of factors acting independently or together. These may include multiple luminescent sites, a high degree of inhomogeneity in the sample, strong electron-phonon coupling, re-absorption of the emitted light by other sites [12, 28, 29].

Typically, when an electron is promoted from the 8s ground state to $^4F_7$ excited states and then into the $^4F_6 \rightarrow {}^5D_1$ excited states, it is most likely that it changes its spin orientation as it now moves downward into low energy level in accordance to *Hund's rule*. Such a transition is also referred to as a spin-forbidden transition. Note, at high energy state the spin of 5D electrons is parallel to the total spin of the 4F core, giving a spin multiplicity equal to sextet or octet. Such a transition provides a high-crystal field effect characterized by a broad emission band at a shorter wavelength such as in this case at 445 nm.

A series of nano phosphor powders were synthesized in which the concentration of activator ion was varied whereas the composition of host matrix, R_o value, synthesis procedure, and sintering temperature were kept unchanged. These samples offered the possibility of studying the effect of dopant ion concentration on PL spectra of the phosphorous material. Fig 13 displays on how the PL spectra of the nanophosphor particles are affected by dopant ion concentration.

It is agreed upon that a critical distance exists between nearby Eu ions above which the effect called concentration quenching is observed. This critical distance is also referred to as the distance between the dopant ion and the quenching site, can be evaluated using $r_c = 2\left(\frac{3V}{4\pi X_c N}\right)^{1/3}$, where V is the volume of the unit cell, X_c is the concentration of Eu, and N is the number of cations per unit cell [30]. The electric multipolar interaction is believed to be the primary mode of non-radiative energy transfer among the Eu ions and is responsible for this concentration quenching. At all compositions, the EDT is more predominant over MDT, which indicates that the majority of Eu ion has asymmetric local surrounding sites.

The intensity of $^5D_o \rightarrow {}^7F_1$ is seen to change with the concentration of Eu ion. The $^5D_o \rightarrow {}^7F_o$ transition is more intense than $^5D_o \rightarrow {}^7F_1$ at 5 % concentration of Eu and this trend seems to reverse at higher compositions/concentrations. With increasing Eu content, the intensity of $^5D_o \rightarrow {}^7F_o$ transition decreases, whereas the strength of $^5D_o \rightarrow {}^7F_1$ increases, likely reduced several oxygen vacancies at higher Eu ion concentration. As the Eu concentration increases, the host-dopant energy transfer efficiency increases, and finally complete transfer is observed at higher concentration.

The intensity of the MDT is independent of the environment in which Eu is located and can be considered on a first approximation to be constant. The MDT is caused by the interaction of the Eu ion with the magnetic field component of the light radiation via magnetic dipole, and it usually occurs as the dipole is displaced over a curved path during the transition.

The MDT shows parity as the rotational symmetry is not reversed under inversion through an inversion center. It means that the MDT possess even transition under inversion and allows transitions between a state with even parity such as intra configurationally transitions $^4F \rightarrow {}^4F$.

Judd-Ofelt method describes the intensities of F→ F intra-band transitions in rare earth. Its appeal lies in the fact that it allows the prediction of oscillator strengths in absorption and luminous bands. (For details on theory, interested readers are referred to elsewhere [31]).

The selection rule for EDT or electric quadrupole transition arises from the displacement of charge that has quadrupole character. It consists of four-point charges with an overall zero charge and zero dipole moment. It is usually considered as two dipole arrangements in a way their dipole moments cancel out. These have even transition parity. These EDTs are much weaker than MDTs and induced electric transitions.

Peer-reviewed version available at Colloids Interfaces 2018, 2, 52; doi:10.3390/colloids2040052

The mixing of charge transfer states is described by selection rule. Since an inverse relation exists between the energy of states of transition and the crystal field strength: low transition energy for charge transfer states results in strong crystal field effects, which enhances orbital mixing.

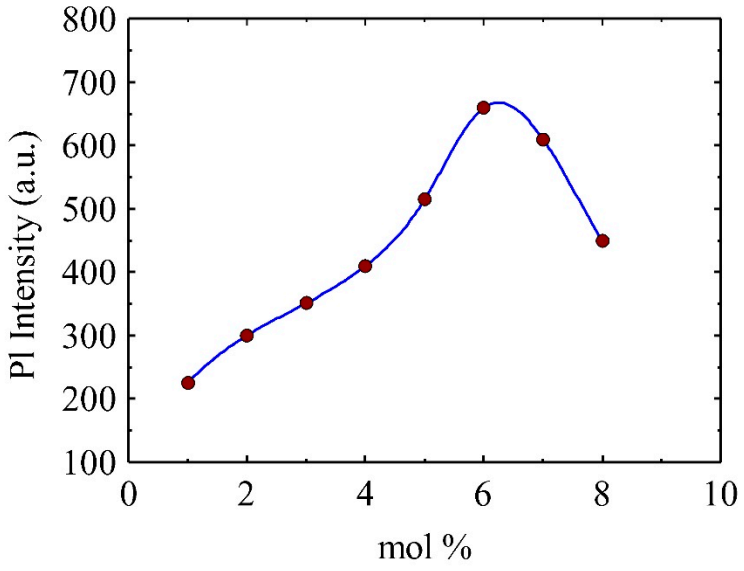

Figure 13. Eu^{3+} ion concentration (mol %) dependence PL spectra of $CaSiO_3$/ SiO_2 nano phosphor powder. Excitation wavelength 220 nm. Samples were prepared using a $R_o = 0.12$ and sintered at 800 ^oC.

Higher intensities are always ascribed to the more ordered crystalline structure, which is believed to give rise to larger linear terms in the crystal field potential.

The intensity of the transition strongly depends on the detail of the crystal size and lattice packing and the interionic distance.

The $^5D_o \rightarrow {}^7F_o$ transition is also useful in the determination of the presence of number of equivalent sites in a host crystal or for the calculation of the number of different Eu species in the matrix because the maximum of one peak is expected of a single site or species due to the non-degeneracy of the ^7F_o and ^5D_o levels.

The appearance of more than one peaks in the spectra of $^5D_o \rightarrow {}^7F_o$ transition is expected, and it means more than one sites or species are present.

The energy difference between two different peaks due to $^5D_o \rightarrow {}^7F_o$ transition are small if the structural difference between these two sites is little and an asymmetric shape of the $5D_o$ only reveals the presence of more than one site $\rightarrow {}^7F_o$ transition line or shoulder. The presence of mixture in the sample means energy difference between the transition.

The $^5D_o \rightarrow {}^7F_1$ transition directly reflects the crystal field splitting of the $^7F_1$ levels. In a cubic or tetrahedral crystal fields, the $^7F_1$ level does not split. In the hexagonal, tetragonal, and trigonal crystal fields, the $^7F_1$ level divides into a non-degenerate and a two-fold degeneracy crystal-field level. In orthorhombic or lower symmetries, the total removal of crystal field degeneracy results in three sub-level of $^7F_1$ states.

The total splitting of the $^7F_1$ level in highly symmetric compounds ranges between 0-1 cm for the cubic phase. Eu compounds with low site symmetry, a large total splitting of $^7F_1$ state can be observed.

The ^5D_o-$^7F_2$ transition is hypersensitive, meaning its intensity and position is strongly influenced by the local symmetry around the Eu^{3+} ion, and it is profoundly affected by the type and nature of the ligands around Eu compared to the intensities of other EDTs.

The results shown in this figure (Fig 13) suggests that, within a specific dopant concentration domain, the PL peak at the vicinity of 610 nm increases with increasing dopant ion concentration. However, when the dopant ion concentration increases beyond a specific threshold concentration, the luminescence intensity started decreasing. Such a decrease in emission intensity as a function of dopant concentration is explained through the so-called quenching effect. It is most likely that, at high concentration, the Eu^{3+} ions may get clustered, and in which case neighboring Eu^{3+} ions would probably quench the energy of the electronically excited Eu^{3+} ion before it gets deactivated through emission, leading to a reduction in emission intensity.

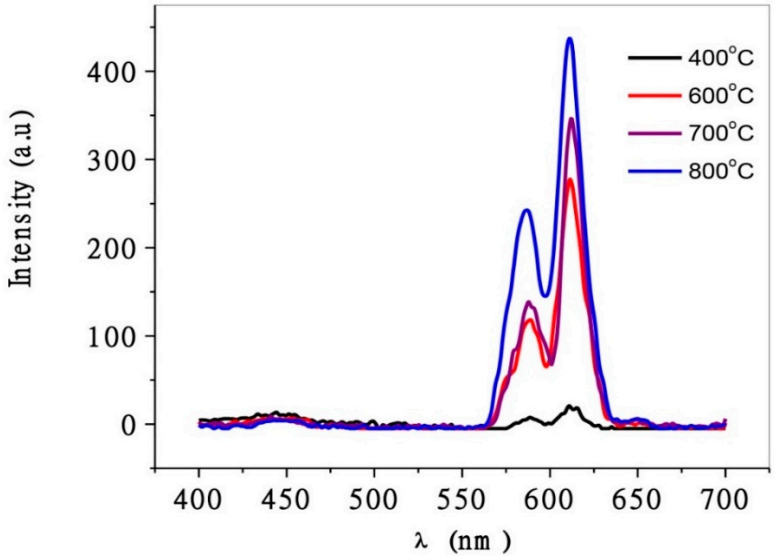

Figure 14. Sintering temperature dependence excitation spectra of Eu^{3+} doped $CaSiO_3$/ SiO_2 nanophosphor powder (λ = 400 to 700 nm). The concentration of Eu^{3+} = 5 mol %; sample was prepared using a R_o value of 0.12.

A series of nanophosphor powders were synthesized under identical R_o value in which the concentration of activator ion and host matrix were maintained constant whereas the resulting powders were sintered at a different temperature. Fig 14 shows on how the PL spectra of these nanophosphor powders are influenced by sintering temperature. As can be seen, the intensity of emission bands increased with sintering temperature. Sample sintered at 400 ^oC gave the lowest emission intensity probably due to its amorphous nature. This figure further suggests that emission bands at 610 nm and 590 nm are strongly related to the sintering temperature and crystal structure. Emission intensity centered at both 610 nm and 580 nm increased with firing temperature, probably suggesting the fact that more defined crystal structures evolve and develop in these samples as a function of sintering temperature.

As shown in it, as the sintering temperature is raised to 800 ^oC, the red emission bands became stronger (with no apparent splitting of the 580 nm band). The emission band at 610 nm, which corresponds to electrical dipole transitions, is stronger than that at 580 nm, a shift corresponding to a magnetic dipole. This may suggest why the Eu^{3+} site symmetry has no center of inversion in Eu^{3+} ion doped $CaSiO_3$ powder.

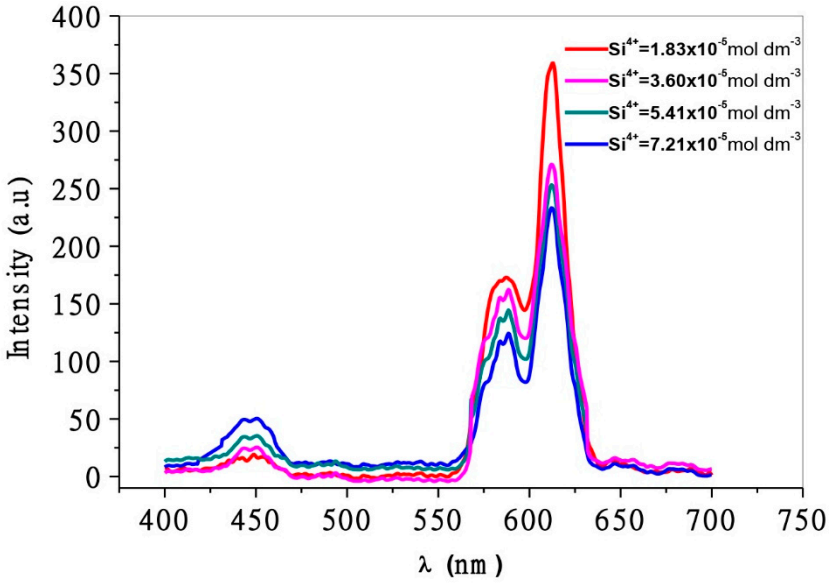

Figure 15. Effect of silica concentration on PL spectra of Eu^{3+} doped $CaSiO_3$ / SiO_2 nano phosphor powder, prepared using $R_o = 0.12$, with a Eu^{3+} ion concentration of 5 mol % and sintered at 800 ^{0}C.

A series of samples were prepared in which the silica concentration was varied while the concentrations of activator and alkali earth ions, R_o value and firing temperature were maintained constant. This series of samples offered the possibility of studying the effect of silica concentration on PL spectra of the given phosphor. As shown in Fig 15, the emission peak intensity at 610 nm increased significantly with decreasing silica concentration, whereas the intensity of the emission band at 440 nm increased with increasing silica concentration. The result suggests that the activation energy of Eu3+ ion reduces with increasing silica concentration, and perhaps it has something to do with a crystallinity of the sample as the degree of crystallinity enhances with the increase in silica concentration.

The effect of Ca^{2+} ion concentration on emission spectra of Eu^{3+} doped $CaSiO_3$nanophospor is given in Fig 16. As can be seen, the intensity of the red emission band has increased with increasing Ca^{2+} concentration and past 2.0 mol %, concentration the emission intensity dropped dramatically.

It seems that Ca^{2+} ion is deficient at low concentration of 1.08×10^{-4} mol dm^{-3} and this leads to the formation of vacant sites not only at Ca^{2+} ions sites but also at those of oxygen ion sites in the conduction plane where charge transfer takes place. The vacancies created at oxygen sites, in turn, can capture electrons, as electron centers at large oxide gaps usually create UV-color centers. And, these color centers provide absorption sites for UV photons and thus compete with activator ions.

On the other hand, at higher Ca^{2+} ion concentration ($Ca^{2+} = 5.41 \times 10^{-4}$ mol dm^{-3}), it is evident that Ca^{2+} ions are in excess in lattice sites. It, in turn, means that Eu^{3+} ions can no longer be able to occupy most cation sites. This situation, in which the crystal lattice contains an excess of Ca^{2+} ion, naturally causes a decrease in emission intensity of bands at 580 nm and 610 nm, due mainly to the loss of sufficient excitation centers and thus excitation energy.

The fact that the intensity of $^5D_o \rightarrow {}^7F_2$ at 611 nm is stronger than $^5D_o \rightarrow {}^7F_1$ at 587 nm is an indication that the local symmetry around Eu is low and deviates from an inversion center.

The coordination number of Ca and Si are 8 and 6 respectively, and their ionic radii are 111 pm and 72 pm, the ionic radii of 8 and 6 coordinated Eu ion are 107 pm and 95 pm, that makes Eu closer in size to Ca and it can easily occupy the larger site near Ca site as opposed to Si site.

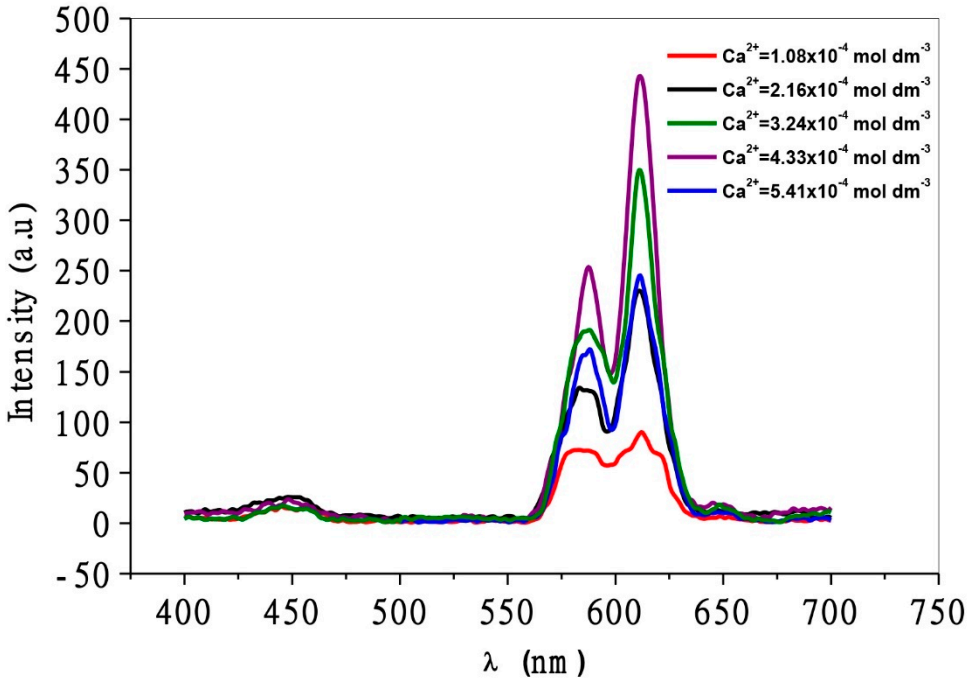

Figure 16. Effect of activator Ion, Ca^{2+} ion, concentration on the emission spectrum of Eu^{3+} doped $CaSiO_3$ / SiO_2 nano phosphor powder. Samples were prepared using $R_o = 0.12$, and with a dopant concentration of 5 mol % and sintered at 800 ^oC.

The charge matching of Eu and Ca allows distortion of the lattice and the associated defects due to the charge size difference is at far off distance, the local site symmetry around Eu occupying Ca will be center of inversion where the smaller chunk holding Ca site will be without inversion symmetry.

The emission spectra where the $^5D_o \rightarrow ^7F_2$ (EDT) at 611 nm of EU is much more intense than the $^5D_o \rightarrow ^7F_1$ (MDT) at 587 nm which can be attributed to the large fraction of Eu occupying Ca sites. Though the oxygen vacancy is introduced in the vicinity to ensure local charge compensation, the presence of MDT is an indication that some of the Eu also occupy Si cites having inversion symmetry.

The fact that ^7F_o and ^5D_o levels are non-degenerate, since both the emitting and end states are non-degenerate, its number of components indicate the number of different metal ion sites. The splitting of $^5D_o \rightarrow ^7F_o$ suggests that an Eu ion occupies two or more non-equivalent sites.

At low doping level concentration (mol %) the $^5D_o \rightarrow ^7F_o$ level do not exhibit a sharp and single peak. However, splitting of it into two components is seen, justifying that the Eu ion is distributed between both the Ca and Si sites.

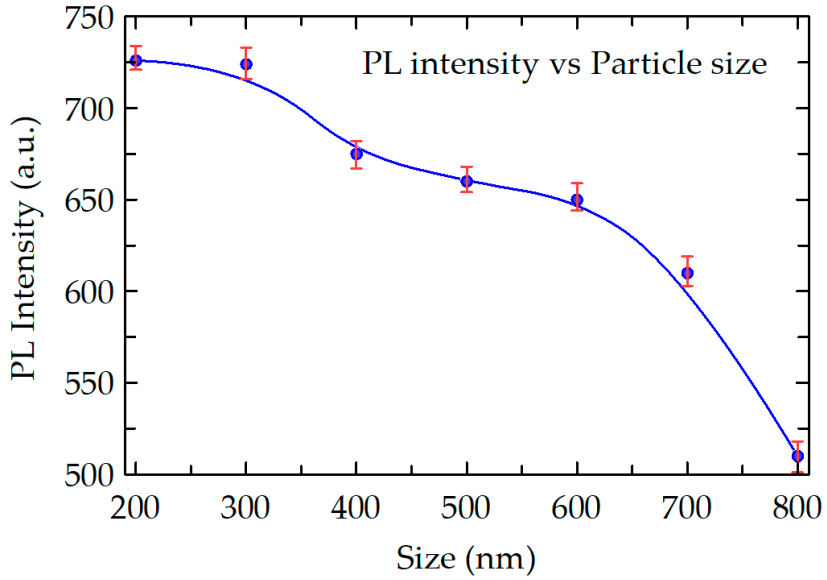

Figure 17. Effect of particle size on emission spectra of Eu^{3+} doped $CaSiO_3$ / SiO_2 nano phosphor, prepared with a dopant concentration = 5 mol % and sintered at 800 °C. The average particle size was varied by varying R_o value of the emulsion system during the preparation. The curve was fitted with B-Spline fit (Open parametric B-Spline curve with data as control points).

In this case, a series of nanophosphor powders with varying average particle size were synthesized by changing R_o value of the emulsion, whereas the concentration of reactants, fabrication procedure, and sintering temperature was kept constant that offers the possibility of exploring particle size dependent PL property of the given phosphor. As shown in Fig 17 the emission intensity due to the nano phosphor powder decreased with increasing particle size, clearly suggesting the fact that the emission efficiency of this phosphor can be enhanced by controlling average size of particles of which it is made up: the emission efficiency can be enhanced by reducing average particle size. Note the average size of the particle in its turn can be controlled by varying the R_0 value of the emulsion during preparation.

5. Conclusions

In the presence of Ca^{2+} ion as a sensitizer Eu^{3+} doped $CaSiO_3$ / SiO_2 nanophosphor showed remarkable photoluminescence, PL property- including – 100 % photon conversion efficiency and a two-fold increase in some excitation and emission photons. It is found that the emission intensity of the given nanophosphor can be enhanced by controlling over average size of the grain of which it is made, and by optimizing chemical composition of sensitizer ion, activator ion, and host matrix ion. The intensity of orange emitting bands at 580 nm and red band at 600 nm has been increased by reducing the grain size of the crystalline powder. The average size of the nanophosphor powder was controlled by controlling the R_o value of the emulsion system: by decreasing the R_o value from 0.3 to 0.12, a dramatic reduction in particle size is achieved. Secondly, the particle size was controlled by controlling sintering temperature: by increasing sintering temperature from 400 °C to 800 °C a substantial increase in particle size and better-ordered crystal phase was achieved. The crystal structure was strongly affected by the sintering temperature. Activator ion concentration showed a strong effect in PL bands, with increasing Ca^{2+} ion the intensity of the red PL band, also referred to as emission bands, increased significantly. Higher concentration of Ca^{2+} showed concentration quenching effect. Si^{4+} ion concentration showed a substantial impact on both the blue and red emission bands: Increase in Si ion concentration lead to decrease in intensity of red PL band centered at 610 nm and 580 nm whereas the intensity of the blue PL band increased with increasing Si^{4+} ion concentration. With increasing Eu^{3+} ion concentration the red emission band initially increased significantly whereas a strong concentration quenching is observed past 2.0 mol %.

Author Contributions: B.N. prepared samples, experimented, and analyzed results and wrote the paper. Both B.N. and C.R. read and approved the article.

Funding: This research received no external funding.

Conflicts of Interest: Authors declare no conflicts of interest.

References

1. Sunitha, D., et al., *Thermo, Iono and photoluminescence properties of 100MeV Si 7+ ions bombarded CaSiO 3: Eu 3+ nanophosphor.* Journal of Luminescence, 2012. **132**(8): p. 2065-2071.
2. Guo-Bo, X., *Luminescence and energy transfer in europium and bismuth codoped trisodium yttrium silicates.* Chinese Physics Letters, 2013. **30**(8): p. 087802.
3. Cable, M., D.R. Uhlmann, and N.J. Kreidl, *Glass: Science and Technology*. 1984.
4. Hryciw, A., et al., *Effects of particle size and excitation spectrum on the photoluminescence of silicon nanocrystals formed by ion implantation.* Nuclear Instruments and Methods in Physics Research Section B: Beam Interactions with Materials and Atoms, 2004. **222**(3): p. 469-476.
5. Hazarika, S. and S. Rai, *Characteristics of Nd 3 ions in solâ€"gel derived silicate glass in presence of Al (NO 3) 3 and the 4 F 3/2â†' 4 I 11/2 transition.* Optical Materials, 2007. **30**(3): p. 462-467.
6. Dhoble, S.J., N.S. Dhoble, and R.B. Pode, *Preparation and characterization of Eu3 activated CaSiO3,(CaA) SiO3 [A= Ba or Sr] phosphors.* Bulletin of Materials Science, 2003. **26**(4): p. 377-382.
7. Terraschke, H. and C. Wickleder, *UV, Blue, Green, Yellow, Red, and Small: Newest Developments on Eu2 - Doped Nanophosphors.* Chemical reviews, 2015. **115**(20): p. 11352-11378.
8. Kimura, I., et al., *Preparation of titania/silica composite microspheres by solâ€"gel process in reverse suspension.* Materials Research Bulletin, 2003. **38**(4): p. 585-597.
9. Nagabhushana, H., et al., *Synthesis, characterization and photoluminescence properties of CaSiO 3: Eu 3 red phosphor.* Spectrochimica Acta Part A: Molecular and Biomolecular Spectroscopy, 2011. **78**(1): p. 64-69.
10. Yamane, M. and Y. Asahara, *Glasses for photonics*. 2000: Cambridge University Press.
11. Barry, T.L., *Equilibria and Eu2 Luminescence of Subsolidus Phases Bounded by Ba3MgSi2 O 8, Sr3MgSi2 O 8, and Ca3MgSi2 O 8.* Journal of the Electrochemical Society, 1968. **115**(7): p. 733-738.
12. Kim, Y.-I., et al., *Combined Rietveld refinement of BaMgAl 10 O 17: Eu 2 using X-ray and neutron powder diffraction data.* Journal of Luminescence, 2002. **99**(2): p. 91-100.
13. Schmechel, R., et al., *Luminescence properties of nanocrystalline Y2O3: Eu3 in different host materials.* Journal of Applied Physics, 2001. **89**(3): p. 1679-1686.
14. Poort, S.H.M., et al., *Luminescence of Eu 2 in silicate host lattices with alkaline earth ions in a row.* Journal of Alloys and Compounds, 1996. **241**(1): p. 75-81.
15. Blasse, G. and B.C. Grabmaier, *Energy Transfer*, in *Luminescent Materials*. 1994, Springer. p. 91-107.
16. Logunov, S., et al., *Interfacial carriers dynamics of CdS nanoparticles.* The Journal of Physical Chemistry A, 1998. **102**(28): p. 5652-5658.
17. Su, Q., J. Lin, and B. Li, *A study on the luminescence properties of Eu 3 and Dy 3 in M 2 RE 8 (SiO 4) 6 O 2 (M= Mg, Ca; RE= Y, Gd, La).* Journal of Alloys and Compounds, 1995. **225**(1): p. 120-123.
18. Leonyuk, N.I. and L.I. Leonyuk, *Growth and characterization of RM 3 (BO 3) 4 crystals.* Progress in crystal growth and characterization of materials, 1995. **31**(3): p. 179-278.
19. Zhang, H.X., et al., *Deposition and photoluminescence of solâ€"gel derived Tb 3 : Zn 2 SiO 4 films on SiO 2/Si.* Thin Solid Films, 2000. **370**(1): p. 50-53.
20. Reisfeld, R. and C.K. JÃ¸rgensen, *Excited state phenomena in vitreous materials.* Handbook on the physics and chemistry of rare earths, 1987. **9**: p. 1-90.

21. Dieke, G.H., H.M. Crosswhite, and H. Crosswhite, *Spectra and energy levels of rare earth ions in crystals*. 1968: Interscience Publishers New York.
22. Carnall, W.T., P.R. Fields, and K. Rajnak, *Electronic energy levels in the trivalent lanthanide aquo ions. I. Pr3 , Nd3 , Pm3 , Sm3 , Dy3 , Ho3 , Er3 , and Tm3*. The Journal of chemical physics, 1968. **49**(10): p. 4424-4442.
23. Lin, Y., et al., *Preparation of the ultrafine SrAl 2 O 4: Eu, Dy needle-like phosphor and its optical properties*. Materials Chemistry and Physics, 2000. **65**(1): p. 103-106.
24. Tallant, D.R., C.H. Seager, and R.L. Simpson. *Mechanisms affecting emission in rare-earth-activated phosphors*. in *MRS Proceedings*. Cambridge Univ Press.
25. Oomen, E. and A.-M.A. Van Dongen, *Europium (III) in oxide glasses: dependence of the emission spectrum upon glass composition*. Journal of Non-Crystalline Solids, 1989. **111**(2): p. 205-213.
26. Shionoya, S., *Photoluminescence*, in *Luminescence of solids*. 1998, Springer. p. 95-133.
27. Leverenz, H.W. and F. Urbach, *Introduction to the Luminescence of Solids*. Physics Today, 2009. **3**(9): p. 32-33.
28. Ellens, A., et al., *Sm 2 in BAM: fluorescent probe for the number of luminescing sites of Eu 2 in BAM*. Journal of Luminescence, 2001. **93**(2): p. 147-153.
29. Liu, Y.-L. and C.-S. Shi, *Luminescent centers of Eu 2 in BaMgAl 10 O 17 phosphor*. Materials Research Bulletin, 2001. **36**(1): p. 109-115.
30. Gupta, S.K., et al., *Intense red emitting monoclinic LaPO4:Eu3+ nanoparticles: host-dopant energy transfer dynamics and photoluminescence properties*. RSC Advances, 2015. **5**(72): p. 58832-58842.
31. Vega, M., et al., *Structural properties, Judd–Ofelt calculations, and near infrared to visible photon up-conversion in Er 3+/Yb 3+ doped BaTiO 3 phosphors under excitation at 1500 nm*. RSC Advances, 2017. **7**(17): p. 10529-10538.